Accepted Manuscript

Geological Society, London, Special Publications

How wet are shallow granites? An experimental investigation

C. A. Grattoni, L. P. Field, B. W. D. Yardley, A. E. Milodowski, R. Metcalfe, Q. J. Fisher & S. Norris

DOI: https://doi.org/10.1144/gslspecpub2025-21

To access the most recent version of this article, please click the DOI URL in the line above. When citing this article please include the above DOI.

Received 24 March 2025
Revised 26 November 2025
Accepted 6 January 2026

How wet are shallow granites? An experimental investigation

C. A. Grattoni[1], L. P. Field[2], B. W. D. Yardley[1,*], A. E. Milodowski[2], R. Metcalfe[3], Q. J. Fisher[1] and S. Norris[4]

[1]School of Earth and Environment, University of Leeds, Leeds, LS2 9JT, UK
[2]British Geological Survey, Keyworth, Nottingham, NG12 5GG, UK
[3]Quintessa Ltd, The Hub, 14 Station Road, Henley-on-Thames, Oxfordshire RG9 1AY, UK
[4]Nuclear Waste Services, Building 329, Thomson Avenue, Harwell Campus, Didcot, Oxfordshire, OX11 0GD, UK
*Correspondence: b.w.d.yardley@leeds.ac.uk
ORCIDS:

C.A.G. https://orcid.org/0000-0003-4418-2435, L.P.F. https://orcid.org/0000-0002-8747-9901, B.W.D.Y. https://orcid.org/0000-0002-3320-0311, A.E.M. https://orcid.org/0000-0002-5141-5615, R.M. https://orcid.org/0000-0002-7968-346X, Q.J.F. https://orcid.org/0000-0002-2881-7018, S.N. https://orcid.org/0000-0001-9316-2428

Abstract

The water content and porosity of a granite sample have been measured to test the assumption that the porosity in crystalline rocks hosting a waste repository will be water-saturated. Undersaturation would reduce the potential role for Rock Matrix Diffusion and impact on the retention of contaminants. A core was drilled from the Grimsel Test Site, Switzerland, with minimal cooling water, and sealed with a resin coating to preserve its water content. The initial water content, porosity, water saturation and gas permeability were determined by multiple laboratory methods, including measurements under stress to recreate in-situ conditions. The initial water content was c. 0.72 vol. % while total porosity was distinctly higher (c. 1.3 vol. %). Sub-samples separated from the core by chipping had anomalously high porosity. Gas porosity reduces with stress and was used to determine a loading factor. Correcting for 450 m of overlying granite gives a total in-situ porosity of 1.03%, indicating the in-situ porosity was less than 75% saturated. Our results show that the water content and porosity of low-porosity crystalline rocks can be measured separately under in-situ conditions, although the saturation level of the cored region might have changed since construction of the Test Site.

Introduction

Strong igneous and metamorphic crystalline rocks such as granite or gneiss are possible host rocks for deep disposal of radioactive waste. The low permeability of most crystalline rocks is a major contribution to their suitability, but beyond the hand specimen scale they have a dual porosity structure. Spaced fractures provide pathways for groundwater flow (Brace 1980, 1984) while fine matrix pores, many of them microcracks, may retain immobile water. If the matrix porosity is interconnected, it can exchange dissolved species with fracture water by diffusion, despite the lack of advection of the pore water (Neretnieks 1980, Mazurek 2000, Metcalfe et al. 2021). This process is termed Rock Matrix Diffusion (RMD), and if it proves effective it holds out the possibility that any radionuclides (or other deep-buried contaminants) that leak into fracture water could then be dispersed through the surrounding rock mass in matrix pore water, retarding the migration of contaminants through the geosphere. For RMD to be fully effective, matrix pores must be interconnected and saturated with water; if saturation is incomplete or limited to the vicinity of flowing fractures, diffusive transport through the liquid water phase of the rock will be reduced, and contaminant retardation by the rock mass may be much less than anticipated. This is because of the reduced water volume and the disruption of possible diffusion pathways by a gas phase.

It is generally the case that the porosity in crystalline rocks immediately below the water table is water-saturated (White et al 2001) whereas at mid-crustal depths, cooled igneous and metamorphic rocks are dry (Frost & Bucher 1994, Yardley & Valley 1997) because any pore water has been consumed by retrograde hydration reactions. It is clear that pores in granite and related rocks sometimes contain water to depths of hundreds of metres (Waber & Smellie 2008) and that within this pore water there are solute concentration gradients away from major fractures (Waber et al. 2012, Eichinger et al. 2020). The way in which water penetrates crystalline rocks as they are exhumed, is poorly understood, although on a larger scale the importance of fractures is often apparent. Vollbrecht at al. (1991) propose that cooling of a rock will cause microcracks to form. The initial formation of the cracks will create undersaturated pore space simply because there is not sufficient fluid available to fill the pore volume. Further cracks may develop in response to exhumation and tectonic movements. The key factors regarding whether they remain undersaturated are therefore the rate at which external fluids enter the pores at any particular depth and the rate at which pore water is consumed by hydration reactions. Hydration rates of igneous minerals unstable with water at low temperatures are slow but not negligible for geological time scales (Yardley et al 2014), while the rate of penetration of water from the surface will depend on uplift rate and may have been strongly impacted by ice cover in glaciated regions.

Despite the critical role of the degree of saturation, most studies of RMD assume that the matrix porosity of granite and similar crystalline rocks is fully water-saturated at repository depths, as suggested by Neretnieks (1980), without attempting to measure saturation. This assumption is crucial for estimating the retardation that can be achieved by RMD. However, most rocks of high temperature origin contain minerals which are not stable in the presence of water in the upper crust. For example, biotite readily hydrates to chlorite + K-feldspar and crucially only water need appear in the balanced reaction, not dissolved species (Yardley et al 2025). Chlorite and K-feldspar are common secondary minerals lining fractures in granite,

and the immediate wallrocks to fractures in granites may be altered completely, so the mineralogical environment of wet granite fractures is quite different from that of the unaltered granite. Below the weathering zone, granites are often unaltered (White et al 2001), even where they have been exposed and eroded at earlier times in the geological record (e.g. Yardley et al., 2025). The implication is that where primary granite minerals have survived for many millions of years, their matrix porosity was not saturated with water.

If the porosity of a granite mass is not completely saturated with liquid water, the efficiency of RMD to transport aqueous phase contaminants away from fractures into the rock mass is greatly reduced. Not only will the amount of water be diminished, but the presence of gas bubbles in the pore network can reduce the number and cross-sectional area of pathways for diffusion.

In view of the importance of water-saturated porosity for RMD, this study was designed to evaluate whether it is possible to measure the degree of water-saturation of in-situ crystalline rock, rather than rely on an assumption. We have investigated a 300 mm diameter core of Grimsel Granodiorite, specially drilled at Nagra's Grimsel underground laboratory located in the Swiss Alps. Measuring the porosity and water content of crystalline rocks under in-situ conditions is extremely challenging. Porosity is dependent on confining pressure and, for investigations of tight rocks, the effects are significant. Our approach has been to use laboratory measurements, with porosity measured at a range of confining pressures. Much of our methodology is comparable to the approaches used by David et al (2018a,b). An alternative approach (Schild et al 2001, Möri et al. 2021) involves injecting water-miscible resin into the rock in-situ, then overcoring the original injection hole to remove an impregnated sample after the resin had been cured. There are potential uncertainties with both approaches, discussed below. Our work differs from other studies in that we have separately measured pore water content and total porosity on the same sub-samples in order to evaluate the degree to which the porosity was water-saturated. We were specifically concerned with the interconnected matrix porosity of crystalline rock. The core that we sampled did not include fractures, while isolated pores (fluid inclusions) made a negligible contribution to porosity (Yardley et al. 2025). Hence the total porosity investigated here refers to the scale of the sub-samples investigated, selected to be typical of the bulk of the rock mass.

In summary, the pore water content and the saturation of the connected matrix porosity are important parameters for evaluating the potential for retention of radionuclides in crystalline rocks such as granite, but are very difficult to determine. At any one site, it reflects the balance between infiltration of water from nearby fractures and consumption of water by hydration reactions. Many studies have measured porosity in granites and other crystalline rocks, but without separately determining the water content. Here we have attempted to determine the water content, total porosity and gas permeability of a sample extracted from depth, and to evaluate the degree of water-saturation under in-situ conditions.

Sampling

To ensure that that our measurements were as relevant as possible to the conditions around a deep disposal facility, we required a sample that had been specially extracted from an in-situ granite body, away from any flowing fractures and with as little introduction of water during drilling as possible. It had to be immediately preserved in resin to prevent drying-out. Accordingly, we contracted Nagra to supply a core obtained to these specifications from their Grimsel Test Site, located in the Grimsel granodiorite. This body is one of the youngest in the Variscan Aar batholith, emplaced at 297 Ma (Ruiz et al. 2022). Despite the established name, much of the Grimsel body is of granite, while the extensive development of spaced Alpine shear zones, accompanied by partial recrystallization of the rock to produce Alpine greenschist facies assemblages, means that it is better thought of as a metagranite (Goncalves et al. 2012). There has been extensive earlier work on the porosity of the Grimsel Granodiorite and its petrophysical properties at the test site, summarised by David et al (2018a,b) and Mori et al. (2021).

The core was drilled almost horizontally into a tunnel wall and 2 pieces were preserved for use in this study. One piece was extracted from between 4.85 and 5.15 metres along the hole from the tunnel wall (core A, Figure 1A), the other piece was from between 5.30 and 5.75 meters (core B, Figure 1B).

Both pieces of core were immediately preserved after recovery by sealing with Sikadur®-52 resin that becomes viscous after about 15 minutes, thereby minimising any loss of pore water. A second coating of the resin was applied the following day, for extra protection. The sampled rock contains no natural water-conducting fractures, although part of core B intersects a narrow, sub-vertical band of mylonitised granite (Figure 1B). Pieces of core A (Figure 1A) were utilised for Mercury Injection Porosimetry (MICP), Nuclear Magnetic Resonance (NMR) and permeability measurements at the University of Leeds. Core B (Figure 1B) was utilised for petrographic characterisation and gravimetric analysis at BGS Keyworth. Despite the care used in sampling it must be borne in mind that, even at this distance from the tunnel, the sampled volume could have been affected during tunnelling or dried by subsequent ventilation. The tunnel from which the core was taken was constructed in 1983 using blasting, while the core was drilled in 2018, so our results relate to the state of the rocks 5 metres behind the tunnel wall 35 years after excavation. In view of the large core diameter and low porosity, we consider that damage or water ingress during sampling will have been minimal. Sub-samples for study were taken from the core interior.

Petrographic characterisation

The primary mineralogy is dominated by quartz, plagioclase (albite in part) and K-feldspar with around 10% biotite. Discrete ductile shear zones were developed during the Alpine orogeny and localised mid-crustal metamorphism resulted in partial reaction of primary minerals in the affected zones, leading to the development of greenschist facies assemblages with a new, green biotite, chlorite, muscovite and epidote (Goncalves et al. 2012) and some sericitisation and albitisation of plagioclase. There is a pervasive Alpine fabric cutting across the core (Figure 1) and one end of core A is darker and has chlorite, rather than biotite, as the main mafic phase. This dark region appears to be associated with Alpine shearing and is concordant with the pervasive fabric whereas the distinct mylonite band in Core B (Figure 1B) crosscuts the Alpine fabric.

Detailed optical and Backscattered Electron Microscopic (BSEM) petrography was carried out primarily on pieces of Core B. Figure 2A is an optical photomicrograph of granite which is only weakly deformed. The original feldspar grains are well preserved but quartz has extensively recrystallized to a fine granoblastic polygonal texture. In contrast, the adjacent late Alpine mylonitic band (Figure 2C) has porphyroclasts of broken feldspar wrapped in a matrix of finely recrystallized quartz with micas and chlorite. The shear zone feature is also shown in a BSEM image in Figure 2D. It is more altered than the adjacent weakly deformed granite and richer in sheet silicates. Biotite and muscovite are both present and biotite occurs both intergrown with, and replaced by, chlorite. The proportion of chlorite is variable, it is very minor in parts of the core but elsewhere is abundant. Small granules of epidote occur with micas in the shear zone (Figure 2D) and locally fine grained allanite is abundant in the mylonitic bands (Figure 2D, inset). The main interconnected porosity of the weakly deformed granite was imaged by injecting molten Field's metal (melting point 62°C) at c.3.5 MPa pressure into a dried Core A sub-sample (Figure 2 E, F). The interconnected porosity occurs as grain boundary pores and microcracks, along mineral cleavages and as secondary dissolution porosity in altered plagioclase.

Sub-Sampling

Sub-samples were taken from each part of the core. In all cases, care was taken to ensure that the water content was unchanged. Sawing and coring were carried out with a minimal amount of water and surfaces were immediately wiped dry while all sub-samples were immediately stored in plastic bags to avoid evaporative loss. The sub-sampling procedures for each of the sub samples are summarised in Table 1.

Pieces of core A were initially removed with chisel and hammer, and immediately sealed in polyethylene sample bags. Three distinct sets of sub-samples were prepared from Core A for Nuclear Magnetic Resonance (NMR) and other measurements in Leeds. Pieces from the chlorite-rich end of the core (4.85m from the tunnel wall) and from the biotite-rich bulk of the core were separated to provide 2 sub-samples of each type which were further broken up using a hammer and steel plate to 1-20 mm in size. They were immediately placed in self-sealing bags and weighed to ensure that the subsamples did not lose water by evaporation. One further piece of each type was cut with a diamond saw lubricated with water to an approximate plug shape and the surface dried before weighing. A single 25 mm diameter core plug was cut and oven dried for mercury injection porosimetry. A further section across the core was quickly cut and a series of core plugs drilled from it, using minimal water. As soon as the cutting and coring were finished, the surfaces were wiped with adsorbent tissue and the pieces placed in self-sealing bags. Four c.60mm core plugs of 37.7 mm diameter were drilled and used to determine initial water content, porosity, and gas permeability as a function of stress.

One end of core B was cut into three pieces using a diamond saw lubricated with water; after cutting the surfaces were rapidly dried using absorbent tissue and wrapped in cling-film to prevent drying out. One piece was broken in a cleaned jaw cutter, then hammered using a steel plate to produce 6 smaller sub-samples (10-20 mm).

Experimental methods

Initial Water Content and Porosity

The initial water content of the core was measured on sub-samples of both core pieces. The water-filled porosity of Core A sub-samples was investigated using NMR(see also David et al 2018b), while pieces of Core B were investigated by Gravimetry. The sub-samples were then resaturated with water to ensure that all the porosity was filled with water and the water content redetermined to give total porosity under ambient conditions. The difference between measurements of the initial water content and the total porosity is a measure of the degree to which the rock cores were water-saturated when first extracted. Below, we show how total porosity measurements were corrected for in-situ conditions. The results obtained from all the sub-samples are summarised in Table 1.

Gravimetry: Each of the 6 sub-samples of Core B was immediately weighed, then placed under vacuum at 20°C in an Edwards Modulyo vacuum-drier and weighed periodically until their weight stabilised. The vacuum drying extracted most of the water but the sub-samples were then placed in an oven at 105 °C until no further weight loss could be detected. The oven-drying accounted for around 20% of the total weight loss.

After drying and weighing, the sub-samples were resaturated with de-aired distilled water using a vacuum chamber at <10 mbar. The samples were left overnight, then the vacuum chamber was returned to atmospheric pressure. Any remaining surface water on the rock fragments was removed using tissue. In order to convert sample weight to volume a grain density of 2.640 g/cm^3 was used, as determined by Mercury Intrusion Porosimetry (MICP). The water density was assumed to be 1.00 g/cm^3. The measurement error in water content by this technique is < 0.05%.

Nuclear Magnetic Resonance (NMR): Water contents were measured on both cored and crushed sub-samples of Core A. The NMR measurements were performed using a Maran Ultra spectrometer, from Oxford Instruments, operating at 2MHz with a sample probe of 40mm. The Carr-Purcell-Meiboom-Gill (CPMG) pulse sequence (Ronczka & Muller-Petke 2012) was used to obtain a magnetisation decay through a series of spin echoes. It comprises a sequence of pulses flipping the magnetic field with specific waiting times between each pulse. The magnitude of the transverse relaxation (T_2) at time zero (maximum signal size) is proportional to the amount of water present. Further details can be found in Coates et al. (1999). The T_2 distribution was obtained by deconvolution, using software provided (DXP) by Oxford Instruments. The measurement was calibrated using a pycnometer containing glass beads and known amounts of water, with the relative error in water volume less than 1.5%.

The initial water contents of crushed material and sawn and cored plug sub-samples were determined immediately after subsampling. Cored plug GR4 was then immediately measured for gas permeability. The plugs were subsequently oven dried, then re-saturated with water, and their total water pore volume determined by NMR, thus allowing the calculation of their total porosity (Table 1).

Mercury Intrusion Porosimetry (MICP): A Micromeritics Autopore IV 9520 system was used for MICP measurements on a separate 25mm diameter sub-sampled core plug from Core A (Webb 2001). The sub-sample had first been oven-dried. The core was loaded into a glass penetrometer and evacuated, and the penetrometer automatically backfilled with mercury.

The pressure was then increased in stages from 1.5 to 37 psi (255 kPa) in the low-pressure port and up to 60000 psi (414 MPa) in the high-pressure chamber. After reaching each pressure the volume of mercury intruded was recorded. The resolution of the volume intruded is 0.1 microliter and the pressure resolution is less than 0.1% of full scale. The pore throat size distribution, bulk density and grain density, as well as porosity, can all be calculated from the data recorded during the test. A plot of pressure against mercury saturation was used to obtain values of Entry Pressure (the pressure at which mercury begins to enter the pore space) and Threshold Pressure (the pressure at which mercury forms a continuous filament through the rock) (Guise et al 2018).

Porosity measurements under stress

The porosity of unconfined samples is likely to be greater than that of the in-situ rock at depth, but the elastic recovery on unloading can be reversed by confining the sample under stress, with allowance for hysteresis as discussed below. We measured the gas porosity of a dry core plug (GR3) over a range of pressures using a bespoke stressed porosimeter consisting of a helium charged reference cell connected to a core holder. The core is placed in a Hassler-type core holder and confining stress is applied. Helium gas is admitted into the reference chamber at a predetermined pressure. After 5 minutes for pressure equilibration, the pressure is recorded and the gas is then allowed to expand into the core holder containing the sample. The resulting lower pressure is measured after the system has reached a new equilibrium and the pore volume obtained using Boyle's law. This method directly determines pore volumes instead of grain volumes. The reference volumes are first calibrated, yielding the reference upstream and downstream reservoir volumes as well as the sample-associated gas volumes. The relative error in pore volume for this method with the core sizes used here is less than 0.15%.

Gas Permeability

Helium gas permeability was measured on samples GR1, GR3 and GR4 at a range of pore and confining pressures to measure the effects of gas pressure and differential stress on the absolute and effective gas permeability. The measurements were made after the cores had been dried, and so document permeability through the total porosity. The gas permeability of GR4 was also measured previously, immediately after the determination of initial water content by NMR and while it still retained its original pore water, to provide a measure of permeability through that part of the porosity that was not occupied by water.
Gas permeability of the core plugs was determined using a pulse-decay permeameter, which is basically an adaptation of the Brace design (Jones 1997). It can accurately measure gas permeabilities of 0.1 mD to 10 nD at confining pressures up to 35 MPa. The permeability of the sample is calculated from the observed transient pressure decay. The equipment was calibrated using reference core plugs and the relative error is less than 10% in the permeability range of the samples tested.

Results

Initial Water Content

The initial water content was measured on all sub-samples before any further work was undertaken, and the results are included in Table 1. Results from gravimetry and NMR are closely comparable when similar samples are compared. The broken pieces of Core A give very similar NMR results (0.58 vol. % water outside the chlorite-rich zone, 1.05 vol. % within)

to Core B chip sub-samples measured gravimetrically (0.53 – 1.05 vol. % water). The Core A sub-samples that had been sawn or cored give slightly higher values (0.6 – 0.9 vol. % water), although the ranges overlap. The chlorite-rich zone in Core A does appear to have a distinctly higher water content than the rest of the core with over 1 vol. % water.

The T_2 relaxation times extracted from the NMR results is proportional to the size of the water-filled pores. The distributions for the chip samples and cored plugs are shown in Figure 3 and in all cases they indicate that water-containing pores have a bimodal size distribution, with a very similar range of values for both the chlorite-rich zone and the rest of the core. Values of T_2 close to 1000 ms correspond to macropores, likely be cracks (Wu et al. 2021). Most of the pore water is likely to be in these features as shown by the amplitude of the T2 distribution. The sample from the chlorite-rich zone at 4.85 m contains one third of its water in smaller pores, whereas samples from the bulk core (5.15 m) only contain one fifth of the water in small pores. This contrast suggests that the higher water content of the chlorite-rich band is due to the presence of more water-filled small pores.

Porosity

After measurement of initial water content, sub-samples were re-saturated so that the new water content could be determined to provide a measure of total porosity. In addition, the porosity of a separate, smaller plug drilled from Core A was measured by MICP and the porosity of several of the dried, cored plugs was measured by He-porosimetry as a function of stress. The total porosity for the plug samples from Core A, investigated by NMR, is included in Table 1 and values range from 1.09 to 1.40 vol. %, except for the plug of the chlorite-rich zone which has a distinctly higher porosity over 2.0 %. These values are around 40% higher than the original water content. Table 1 also includes the porosity calculated for Core B chip sub-samples following water re-saturation. These values are significantly higher (by a factor of 2 to 3) than the initial porewater content. This difference suggests that the porosity in the chip samples may have increased during break-up of the sample or during drying and re-saturation. As a result, these data are believed to over-estimate the total porosity of the rock, and have therefore been left out of the later interpretation. The distribution of T_2 relaxation times for re-saturated plugs is qualitatively similar to the initial distribution (Figure 3D) but the peak believed to correspond to water in microcracks is larger, suggesting that the additional water that entered during re-saturation almost exclusively entered large pores and microcracks.

The MICP measurements of porosity were carried out using the largest core size that the instrument can accept, but the amount of mercury that could be injected was nevertheless close to the recommended lower limit. This method yielded a porosity of 0.8%, lower than the results from NMR. This apparent discrepancy results in part from the different properties of the different liquids injected, but also reflects the experimental differences and methodology. The sample in the NMR sample holder is unconfined and at ambient pressure, whereas for MICP measurements the mercury compresses the sample until the entry pressure is reached at c. 2MPa, which will tend to close pores, as discussed in the next section. The MICP total porosity is measured at 413 MPa, and in view of these differences, the MICP porosity is considered a reasonable match to the results from NMR.

Pore Size Distribution

The pore size frequency distribution was also obtained from the MICP data and is presented in Figure 4. The majority of pore radii are between 0.01 μm and 0.46 μm with a peak in the distribution corresponding to a pore radius of 0.113 μm. There is a small number of pores above 1 μm, which likely correspond to micro-cracks, with some mercury starting to enter the sample above 172 kPa. However, the Entry Pressure to the main pore size distribution is 2.07 MPa and the Threshold Pressure is approximately 5.52 MPa. It should be noted that the NMR distribution is based on the volume of water in different size pores, whereas the MICP distribution is based on numbers of pores. Thus the sparsity of large pores from Figure 4 is still consistent with a high proportion of the water residing in such pores, as indicated by Figure 3.

Porosity under Stress

The porosity measurements on water-saturated samples were made at ambient conditions and so include additional porosity created in response to unloading. To correct for the effect of loading on porosity, dried sub-sample GR3 was investigated using a helium stressed porosimeter to measure porosity at pressure. Helium was used to determine stress effects rather than water because the time taken for equilibration as the load pressure is changed, is much less. The results are shown in Figure 5 and confirm that the porosity is stress dependant. Under ambient pressure and following an initial loading cycle, the total He porosity is 1.4 %, slightly higher than the volume determined for total water-saturated porosity in the same core (1.28 %). Confining pressure was raised in stages to 24 MPa, leading to a reduction in He-porosity of c.30% to 0.98 %. The depth of the Grimsel site is c. 350 – 520 m so we assumed a typical value of 450 m, corresponding to an in-situ overburden pressure near 11.5 MPa. Figure 5 demonstrates that for plug GR3 the ambient porosity was reduced to 1.1 % under this load, corresponding to a loading factor of 0.79 (Table 2). At no pressure on Figure 5 does the porosity approach the measured water content of this sub-sample (0.76%, Table 1). Applying the same loading factor to all the NMR total porosity data yields in-situ porosity values of 0.86-1.1 vol.%, with a slightly higher value for the chlorite-rich region (1.6 vol. %) (Table 2). It is notable that this corrected porosity is now in better agreement with porosity by MICP, as discussed earlier. To check the validity of applying a loading factor derived using helium, to water-filled cores, we also measured a water-saturated sub-sample, core GR1. The test was performed at a constant pore pressure of 1.4 MPa, while increasing the confining stress. The porosity measured with in-situ loading was within error of the calculated value at 11.5 MPa, reported in Table 2.

Water saturation

The initial water saturation at ambient conditions in the laboratory can be calculated from the initial volume of water divided by the water volume after re-saturation (i.e. total pore volume); the average water saturation for the plugs at ambient pressure (excluding the

chlorite-rich zone) is 59%. This is an underestimate, influenced by cracks opened during sampling, but after correcting the value of total porosity for the pressure at the nominal in-situ depth of 450m (Table 2), saturation is still significantly below 100% (Table 2). The average saturation under in-situ conditions is 73.5%, with a slightly higher value (84%) for the chlorite-rich zone. Thus, while stress relaxation during sampling accounts in part for the undersaturated porosity measured at ambient conditions, the effect is not large enough to account for all the undersaturation observed.

Gas permeability

Helium gas permeability was measured on dried core plugs GR1 and GR3 as a function of gas pressure and confining pressure and the results are presented in Figure 6 as a function of both.

Gas permeability varies with the molecular weight of the gas and the applied gas pressure (P), as a consequence of gas slippage at the pore wall (Rosenbrand et al. 2015; McPhee et al. 2015). To correct for this, the Klinkenberg corrected permeability, kL, which is independent of the gas pressure, was obtained by measuring permeability at several gas pressures, plotting permeability against reciprocal gas pressure (Figure 6), and extrapolating to a reciprocal gas pressure of zero. The effect is important for low-permeability rocks and the value of kL obtained after applying the correction represents the permeability to a gas at infinite pressure (1/P = 0) or to a liquid that does not react with the component minerals of the rock. The value of kL is a function of the confining pressure (see Figure 6). Both the slope and intercept show that the effect of confining pressure on permeability is more important than the slippage effect due to variations in gas pressure.

Gas pressure and confining stress can be combined in one value called net stress, which is defined as the confining pressure minus the gas pore pressure. The permeability, and hence also the dominant pore size, decrease significantly as the net stress increases, but the core retains a measurable gas permeability of 3.5 μD at the maximum confining pressure of 31MPa, which is in excess of the in-situ stress. Stress hysteresis was observed during the initial loading and unloading cycles and is shown for core plug GR1 in Figure 7. Core plug GR3 gave similar results. The initial loading produces a large drop in porosity and permeability which includes closure of microcracks induced during sampling. Subsequent unloading does not reopen these artefacts and the changes correspond to elastic deformation of the minerals. This type of hysteresis is typical of stress relaxation from in-situ to ambient conditions followed by re-stressing the sample. It can be observed that even at 27.5 MPa the gas permeability is 4 μD, which is high for a low porosity matrix and suggests that the flow is dominated by microcracks.

The gas permeability of sample GR4 at initial water content (55 % water saturation at ambient conditions) was also measured as a function of net stress in order to obtain the relative gas permeability (K_{rg}). K_{rg} is a dimensionless measure of the effective permeability of gas through the original, water-bearing sample relative to the gas permeability of the dried rock. This measurement was performed during unloading and the results are shown in Figure 7. Sample GR4 with its initial water content follows the same trend as the dry core

but with a lower gas permeability. Within the stress range tested, the relative gas permeability varies between 0.51 and 0.64. The reduced permeability of the gas phase when the original water remains is typical for two-phase behaviour and provides further evidence that there is a gas flow path available even at higher stresses, demonstrating that the sample is only partially water saturated, even at higher confining pressures than in situ conditions.

Discussion and Conclusions

The results obtained in this study give very consistent estimates for the pore water content of the deep Grimsel granodiorite sample, irrespective of the method of sub-sampling and method of water determination. Except for a chlorite-rich section of core, the water content is in the range 0.54 to 0.90 vol.%, with a mean value of 0.72%. Sub-samples taken by hammering, without any use of water, have slightly lower values than sub-samples that were sawn or drilled with minimal water, but the ranges overlap suggesting very little or no water was introduced in preparation. Similarly, water-loss under vacuum was very slow, with the water content beginning to plateau after 20 hours, and so it is unlikely that there was any significant loss during sample preparation.

The total porosity of the samples, measured after drying and re-saturation with water, was invariably higher than the initial water content, averaging 1.03 vol. % for the sawn or drilled sub samples, although chip samples gave higher values, which is interpreted as a result of damage during sub-sampling. The porosity results for unstressed samples reported here are comparable to those from the KG^2B collaborative benchmarking exercise for the Grimsel granodiorite (David et al 2018b), although the MICP porosity obtained here (0.8%) is slightly higher than their MICP value of 0.6%, while the NMR porosity of biotite granite (1.3%) is similarly higher than the NMR porosity reported by David et al. (2018b). Möri et al. (2021) also obtained an MICP porosity of 0.75% for Grimsel granodorite.

The effects of stress release during sampling have been evaluated by measuring Helium gas porosity at a range of confining pressures to match and exceed the in-situ overburden load. Applying a confining pressure results in a reduction in porosity, and at the in-situ stress the porosity was around 80% of the value measured at ambient laboratory conditions. Our in-situ porosity estimates (Table 2) are significantly larger than those reported by Möri et al. (2021) and Schild et al (2001), also from the Grimsel test site, obtained using in-situ resin injection. Möri et al. (2021) obtained in-situ porosity values of c. 0.3 vol. %, although an MICP porosity measurement on an impregnated specimen yielded a further 0.3% porosity. Schild et al (2001) also reported smaller in-situ porosities than we found, c. 0.6%, but in both cases the measured porosity is less than the volume of water present in our sample. The discrepancy is likely to reflect both the different approaches and lithological variation.

An additional factor for which we have been unable to correct, is stress anisotropy at the test site. Gischig et al (2018) reported that, although the mean stress was close to the value of 11.5 MPa which we have used for calculations of the stress effect, the principal normal stress σ_1 ranged up to 17 MPa. However, since gas porosity and permeability measurements were made to 25 MPa, there are unlikely to be major consequences for the calculated in situ porosity.

After applying a loading factor, the porosity of all our sub-samples is still larger than their measured water content and implies that the porosity was not fully saturated with water at the time the sample was drilled. Instead, the pores are still calculated to be only 65 - 82% saturated with water.

This conclusion is supported by the significant gas permeability determined for a sample measured under stress while the original water content was still present. This result is potentially very significant for RMD, but the long period of time that has elapsed since the construction of the tunnel means that it is not possible to be sure that the granite was also undersaturated when work at the test site started. The years of ventilation of the tunnel might have reduced the pore water content of the granite 5 metres behind the tunnel wall.

The degree of water-saturation in crystalline rocks hosting a waste repository is important for modelling the fate of radionuclides or contaminants that come into contact with them, because the effectiveness of Rock Matrix Diffusion depends on the presence of a continuous film of pore water, and its thickness. If there is gas as well as water in the pore space it will disrupt the continuous water film assumed for RMD. The results reported here show that it is possible to make independent measurements of pore water content and porosity in order to evaluate whether crystalline rocks are water-saturated. With suitable planning, samples can be taken for measurement before the effects of disturbance at a site are likely to have affected the mass of low-permeability rock.

Acknowledgements

We thank S. Allshorn for performing the tests of porosity as a function of stress. L.P. Field and A.E. Milodowski publish with the permission of the Executive Director of the British Geological Survey (UKRI). Nagra are thanked for drilling and preserving the core. The work was funded by Radioactive Waste Management Limited, now Nuclear Waste Services.

References

Brace, W.F. 1980. Permeability of crystalline and argillaceous rocks. *International Journal of Rock Mechanics and Mining Sciences*, **17**, 241-251.

Brace, W.F. 1984. Permeability of crystalline rocks: new in-situ measurements. *Journal of Geophysical Research,* **89(NB6)**, pp.4327-4330. https://doi.org/10.1029/JB089iB06p04327

Coates, G.R. 1999. NMR Logging: Principles and Applications. Elsevier Science, 234pp.

David, C. J. Wassermann, F. *et al.* 2018a. KG^{2}B, a collaborative benchmarking exercise for estimating the permeability of the Grimsel granodiorite – Part 1: measurements, pressure dependence and pore-fluid effects. *Geophysical Journal International*, **215**, 799–824. doi: 10.1093/gji/ggy304

David, C. J. Wassermann, F. *et al.* 2018b. KG^{2}B, a collaborative benchmarking exercise for estimating the permeability of the Grimsel granodiorite – Part 2: modelling, microstructures and complementary data. *Geophysical Journal International*, **215**, 825-843. doi: 10.1093/gji/ggy305

Eichinger, F., Gimmi, T., Möri, A. and Rüedi, J. 2020. Profiles of chloride in matrix porewater as natural tracer for matrix diffusion in crystalline rocks. *Applied Geochemistry*, **118**, 104635. https://doi.org/10.1016/j.apgeochem.2020.104635

Frost, B.R. and Bucher, K. 1994. Is water responsible for geophysical anomalies in the deep continental crust? – A petrological perspective. *Tectonophysics*, **231**, 293-309. https://doi.org/10.1016/0040-1951(94)90040-X

Gischig, V.S., Doetsch, J., *et al.* 2018. On the link between stress field and small-scale hydraulic fracture growth in an isotropic rock derived from microseismicity. *Solid Earth*, **9**, 39–61. https://doi.org/10.5194/se-9-39-2018

Goncalves, P., Oliot, E., Marquer, D. and Connolly, J.A.D. 2012. Role of chemical processes on shear zone formation: an example from the Grimsel metagranodiorite (Aar massif, Central Alps). *Journal of Metamorphic Geology*, **30**, 703-722. https://doi.org/10.1111/j.1525-1314.2012.00991.x

Guise, P.G., Grattoni, C., Allshorn, S., Fisher, Q.J. and Schiffer, A. 2018. Stress Sensitivity of Mercury-Injection Measurements. *Petrophysics*, **59**, 25-34. https://doi.org/10.30632/PJV59N1-2018a2

Jones, S.C. 1997. A technique for faster pulse-decay permeability measurements in tight rocks. *Society of Petroleum Engineers Formation Evaluation*, **12**, 19-26. https://doi.org/10.2118/28450PA

Mazurek, M. 2000. Geological and hydraulical properties of water-conducting features in crystalline rocks. *In* Stober, I. and Bucher, K. (eds) *Hydrogeology of Crystalline Rocks*. Kluwer Academic Publishers, 3–26. https://doi.org/10.1007/978-94-017-1816-5_1

McPhee, C., Reed, J. and Izaskun Zubizaretta, J.-R. 2015. Core analysis: a best practice guide. Developments in Petroleum Science **64**, Elsevier. ISBN: 9780444635334.

Metcalfe R., Milodowski A.E., Field, L.P., Wogelius R.A., Carpenter G., Yardley B.W.D. and Norris S. 2021. Natural analogue evidence for controls on radionuclide uptake by

fractured crystalline rock. *Applied Geochemistry*, **124**, 104812, https://doi.org/10.1016/j.apgeochem.2020.104812.

Möri, A., Mazurek, M., Ota, K., Siitari-Kauppi, M., Eichinger, F. and Leuenberger, M. 2021. Quantifying the porosity of crystalline rocks by in-situ and laboratory injection methods. *Minerals*, **11**, 1072. https://doi.org/10.3390/min11101072

Neretnieks, I. 1980. Diffusion in the rock matrix: An important factor in radionuclide retardation? *Journal of Geophysical Research*, **85**, 4379–4397. https://doi.org/10.1029/JB085iB08p04379

Ronczka, M. and Muller-Petke, M. 2012. Optimization of CPMG sequences to measure NMR transverse relaxation time T2 in borehole applications. *Geoscientific Instrumentation, Methods and Data Systems*, **1**, 197-208. https://doi.org/10.5194/gi-1-197-2012

Rosenbrand, E., Fabricius, I.L., Fisher, Q. and Grattoni, C.A. 2015. Permeability in Rotliegend gas sandstones to gas and brine as predicted from NMR, mercury injection and image analysis. *Marine and Petroleum Geology*, **64**, 189-202. https://doi.org/10.1016/j.marpetgeo.2015.02.009

Ruiz, M., Schaltegger, U., Gaynor, S.P., Chiaradia, M., Abrecht, J., Gisler, C., Giavanoli, F. and Wiederkehr, M. 2022. Reassessing the intrusive tempo and magma genesis of the late Variscan Aar batholith: U– Pb geochronology, trace element and initial Hf isotope composition of zircon. *Swiss Journal of Geosciences*, **115**, 20-24. https://doi.org/10.1186/s00015-022-00420-1

Schild, M., Siegesmund, S., Vollbrecht, A. And Mazurek, M. 2001. Characterization of granite matrix porosity and pore-space geometry by in situ and laboratory methods. *Geophysical Journal International*, **146**, 111–12. Vollbrecht, A., Rust, S. and Weber, K. 1991. Development of microcracks in granites during cooling and uplift: examples from the Variscan basement in NE Bavaria, Germany. *Journal of Structural Geology*, **13**, 787-799. https://doi.org/10.1016/0191-8141(91)90004-3

Waber, H.N. and Smellie, J., 2008. Characterisation of pore water in crystalline rocks. *Applied Geochemistry*, ***23***, 1834–1861. http://dx.doi.org/10.1016/j.apgeochem.2008.02.007

Waber, H.N., Gimmi, T. and Smellie, J.A.T. 2012. Reconstruction of palaeoinfiltration during the Holocene using porewater data (Laxemar, Sweden). Geochimica et Cosmochimica Acta, **94**, 109–127. https://doi.org/10.1016/j.gca.2012.06.030

Webb, P. A. 2001. An introduction to the physical characterization of materials by mercury intrusion porosimetry with emphasis on reduction and presentation of experimental data. Technical Note, Norcross, GA, Micromeritics Instrument Corporation.

White, A.F., Blum, A.E., Stonestrom, D.A., Bullen, T.D., Schulz, M.S., Huntington, T.G. and Peters, N.E. 2001. Differential rates of feldspar weathering in granitic regoliths. Geochim. Cosmochim. Acta 65(847–869): 37–59.

Wu, X., Guo, Q. *et al*. 2021. Pore structure and crack characteristics in high-temperature granite under water-cooling. *Case Studies in Thermal Engineering*, **28**, 101646. https://doi.org/10.1016/j.csite.2021.101646

Yardley, B.W.D. and Valley, J.W. 1997. The petrologic case for a dry lower crust. *Journal of Geophysical Research*, **102**, 12173-12185. https://doi.org/10.1029/97JB00508

Yardley, B.W.D., Rhede, D. and Heinrich, W., 2014. Rates of retrograde metamorphism and their implications for the rheology of the crust: an experimental study. *Journal of Petrology*, **55**, 623-641. https://doi.org/10.1093/petrology/egu001

Yardley, B.W.D., Wogelius, R. *et al*. (2025). Penetration of groundwater into crystalline rocks. *Hydrogeology Journal*, https://doi.org/10.1007/s10040-025-02906-2.

Figure Captions

Figure 1. Images of the pieces of core used in this study. The sheen is due to the resin coating. A) Core A, weakly foliated biotite granodiorite with a dark band to the right parallel to the foliation which is rich in chlorite as a result of Alpine greenschist facies metamorphism. B) Core B, foliated biotite granodiorite cut by late Alpine shear zones (dark lines).

Figure 2. Petrography of the granodiorite core. A) Optical photomicrograph (cross polarised light) of little-deformed granite. Large grains are mainly igneous feldspars (fsp1) while original quartz (qz1) has partially recrystallized to a fine mortar (qz2). B) Optical photomicrograph (cross polarised light) of deformed granite from a mylonitic band with feldspar remnants now forming porphyroclasts (fsp1), wrapped around by finely recrystallized quartz (qz2) and sheet silicates (chl). C) BSEM image of little-deformed granite with primary K-feldspar (Kf), albite (ab) and biotite mica (bio). Grains of secondary epidote (ep) occur in the mica. D) BSEM image of altered and deformed shear zone granite. Intergrown albite (ab) and quartz (qz) appear dark grey, K-feldspar (Kf) and mica appear mid grey and are heavily speckled with white grains oepidote (ep) and allanite (all). The inset is a detail showing small granules of allanite in a dark matrix of chlorite with bright cores rich in cerium (Ce-all). E, F) BSEM image of granite injected with Field's metal to highlight the presence of porosity. E) displays grain boundary porosity around quartz (qz), itself cutting perthitic K-feldspar (Kf and ab). F) is an example of microcrack porosity cutting perthitic K-feldspar.

Figure 3. The distribution of T_2 relaxation times obtained by NMR for sub-samples from Core A (Table 1). The water signal is dependent on sample size, therefore to compare different

sub-samples in parts A and B the Y-axis been normalised to the total amount of water. In parts C and D each plot shows results from a single sub-sample, hence the measured water content is shown as the sample size remains constant. A) Chip sub-samples with separate curves for the main part of the core and for the chlorite-rich part. B) Core plugs GR1 – GR4, all measured immediately after coring. C),D) Core plugs GR1 and GR4 contrasting the original distribution from part B with the distribution after re-saturation.

Figure 4. Pore size distribution in the 25mm diameter cored plug investigated by MICP. Incremental intrusion is the volume of mercury injected between two consecutive pressure steps (mm^3/g). The larger pores (>1μm) likely correspond to microcracks.

Figure 5. He-porosity of cored plug GR3, measured on the dried core as a function of confining pressure. The depth from which the cores were removed was c. 450m, corresponding to an overburden pressure of 11.5 MPa.

Figure 6. Plot of the gas permeability of sub-sample GR1 as a function of gas pressure at 3 different confining pressures, measured during progressive unloading. Curves are extrapolated to infinite gas pressure at the y-axis to obtain the Klinkenberg permeability.

Figure 7. Gas permeability as a function of net stress during loading and unloading for cored plug GR1, measured dry at an average gas pressure of 1.90 MPa.

Figure 8. Klinkenberg corrected permeability as a function of net stress during unloading for sample GR4 with the original water content and after drying. The significant gas permeability at in-situ stress (c. 11.5 MPa) and with the original water content demonstrates that the pores were not fully saturated with water.

Table Captions

Table 1. Measurements of the pore water content of the Grimsel Granite sub-samples, as sampled and after resaturation at ambient conditions.

Table 2. Total porosities of Core A samples, corrected for 450m overburden pressure, and resultant pore water saturation in-situ.

Sub-sample type	Core	Sub-sample	Measured by	Initial water (vol.%)	Resaturated water (vol.%)	% Saturation ambient P
Chips	A	Bi-gte $_1$	NMR	0.62	-	
Chips	A	Bi-gte $_2$	NMR	0.54	-	
Chips	A	Chl-gte $_1$	NMR	1.04	-	
Chips	A	Chl-gte $_2$	NMR	1.06	-	
Chips	B	Bi-gte α_1	Grav.	0.76	*2.22*	*34.23*
Chips	B	Bi-gte α_2	Grav.	0.74	*2.22*	*33.33*
Chips	B	Bi-gte β_1	Grav.	1.05	*2.47*	*42.51*
Chips	B	Bi-gte β_2	Grav.	0.63	*2.19*	*28.77*
Chips	B	Bi-gte γ_1	Grav.	0.53	*1.94*	*27.32*
Chips	B	Bi-gte γ_2	Grav.	0.60	*1.89*	*31.75*
Sawn Plug	A	Chl-gte C2	NMR	1.35	2.05	65.85
Sawn Plug	A	Bi-gte C1	NMR	0.61	1.09	55.96
Sub-Core	A	Bi-gte GR1	NMR	0.90	1.40	64.29
Sub-Core	A	Bi-gte GR2	NMR	0.88	-	
Sub-Core	A	Bi-gte GR3	NMR	0.76	1.28	59.38
Sub-Core	A	Bi-gte GR4	NMR	0.75	1.46	51.37
Means						
	A	Bi-gte	NMR	0.72	1.31	57.75
		n		7	4	
	A	Chl-gte	NMR	1.15	2.05	65.85
		n		3	1	
	B	Bi-gte	Grav.	0.72	*2.16*	*32.99*
		n		6	6	6
Data in greyed italics has been rejected (see text).						
Abbreviations: Grav. = Gravimetry, NMR = Nuclear Magnetic Resonance, Bi-gte = Biotite granite, Chl-gte = Chlorite granite.						

Table 1

Pore Fluid:	He-gas	water					Mean water porosity
sub-sample:	GR3	C1	C2 (chl)	GR1	GR3	GR4	Bio-gte
Porosity at ambient pressure (vol. %)*							
	1.40	1.09	2.05	1.40	1.28	1.46	1.31
Porosity at 11.5MPa (vol. %)							
	1.10						
Loading factor†	0.79						
Porosity calculated at 11.5MPa (vol. %)‡							
		0.86	1.61	1.10	1.01	1.15	1.03
In-situ Saturation (%)§		71.2	83.8	81.8	75.6	65.4	73.50
* resaturated water porosity from Table 1							
† He porosity at 11.5 MPa / He porosity at ambient P							
‡ measured porosity times loading factor							
§ initial water porosity / calculated resaturated water porosity							
Abbreviations as in Table 1							

Table 2

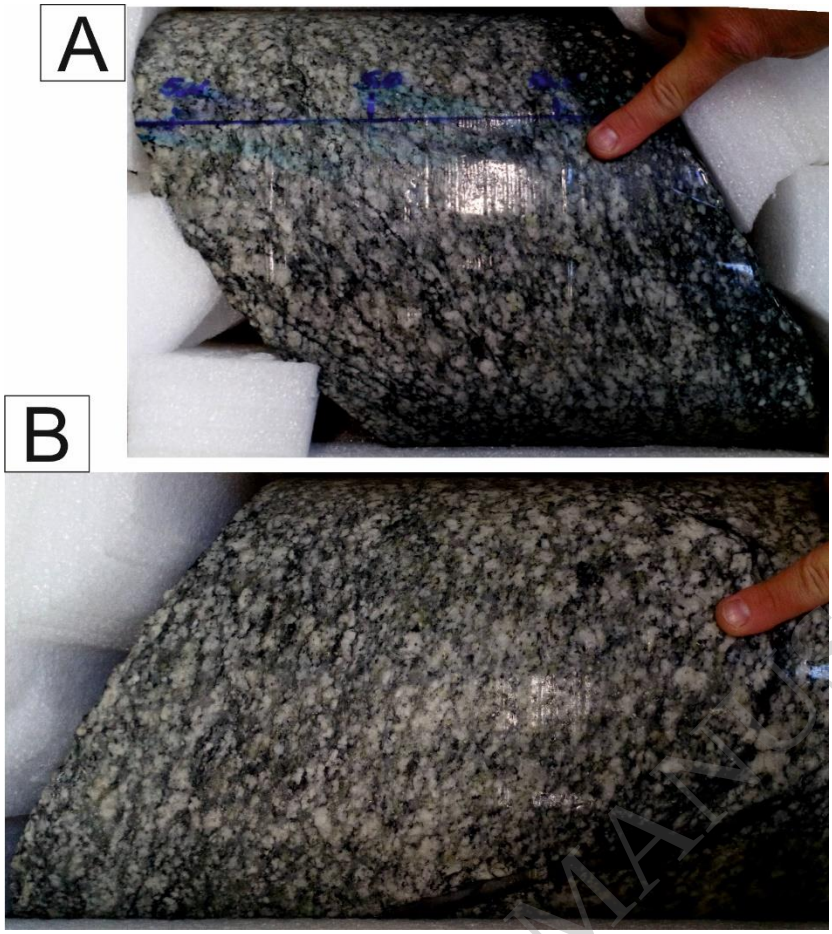

Figure 1

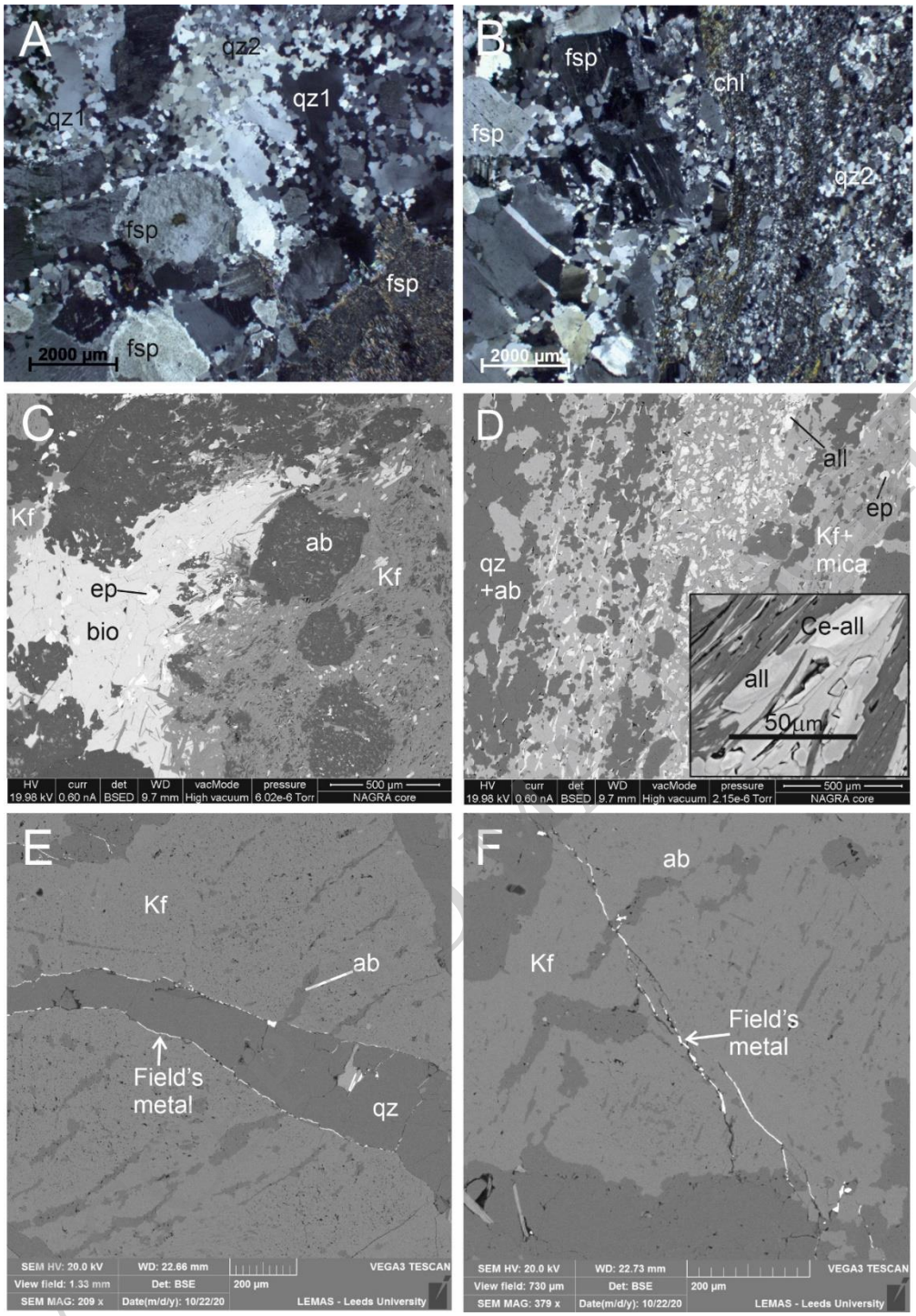

Figure 2

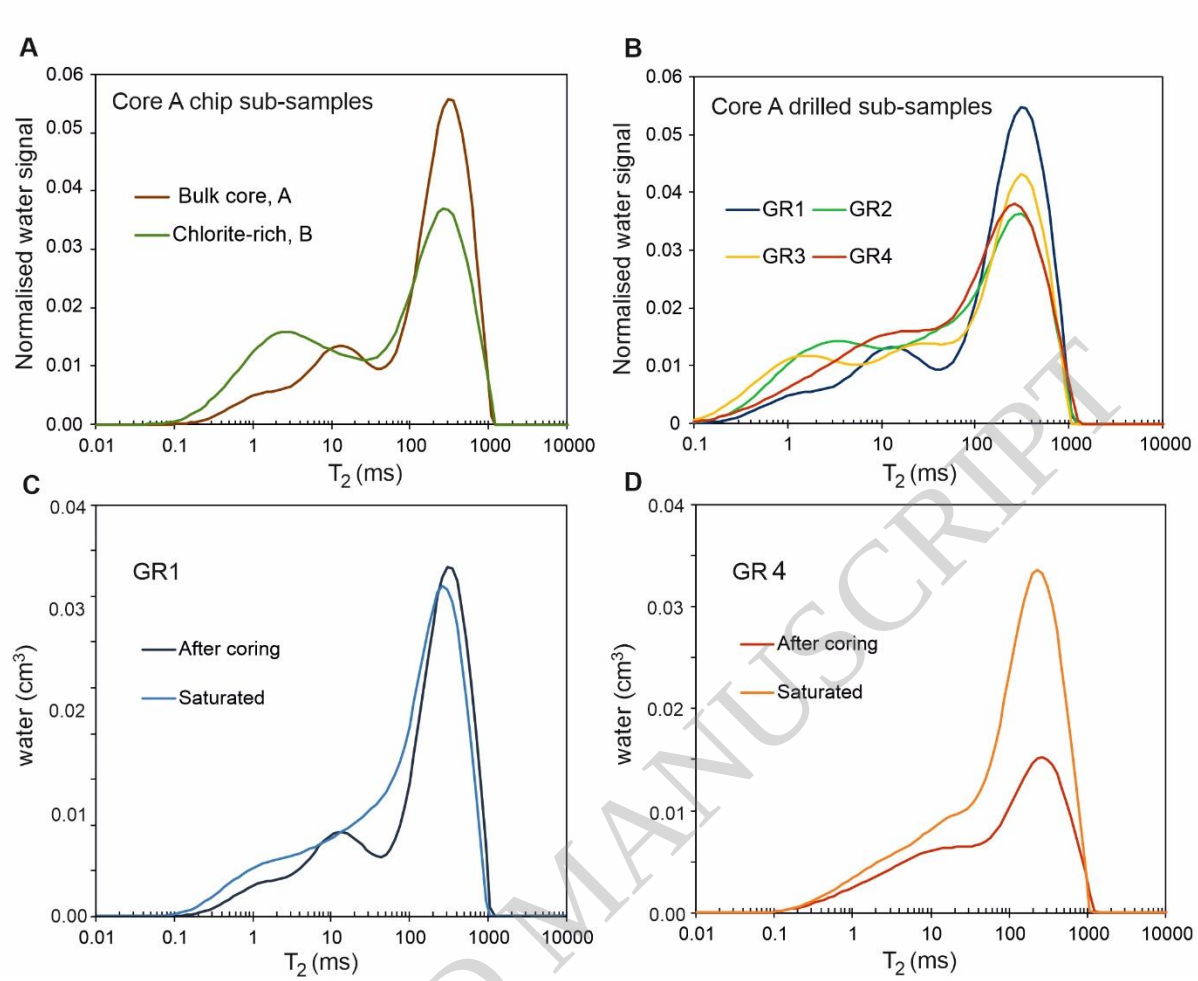

Figure 3

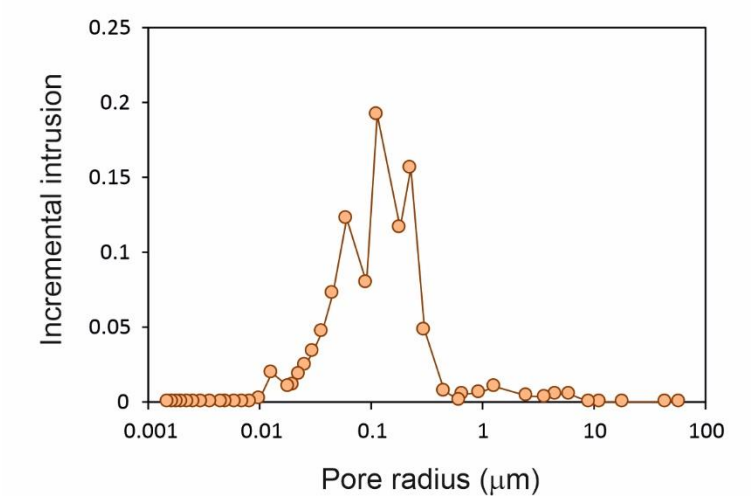

Figure 4

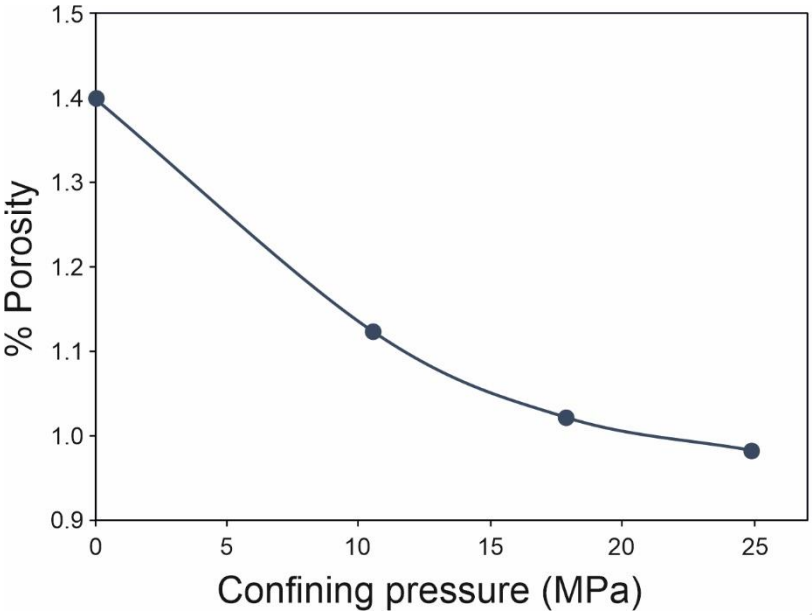

Figure 5

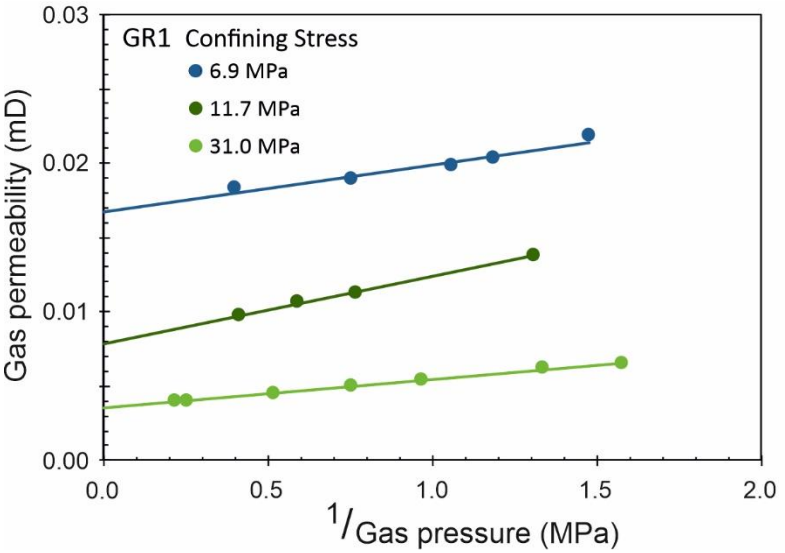

Figure 6

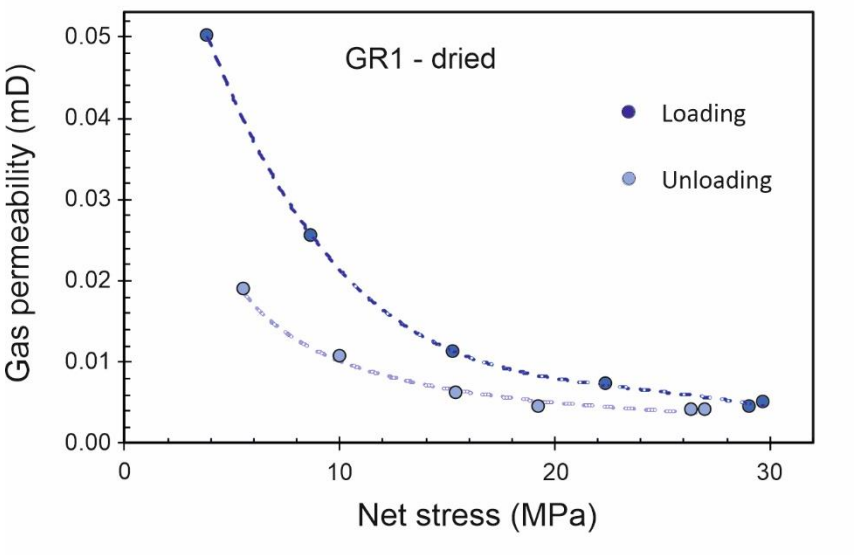

Figure 7

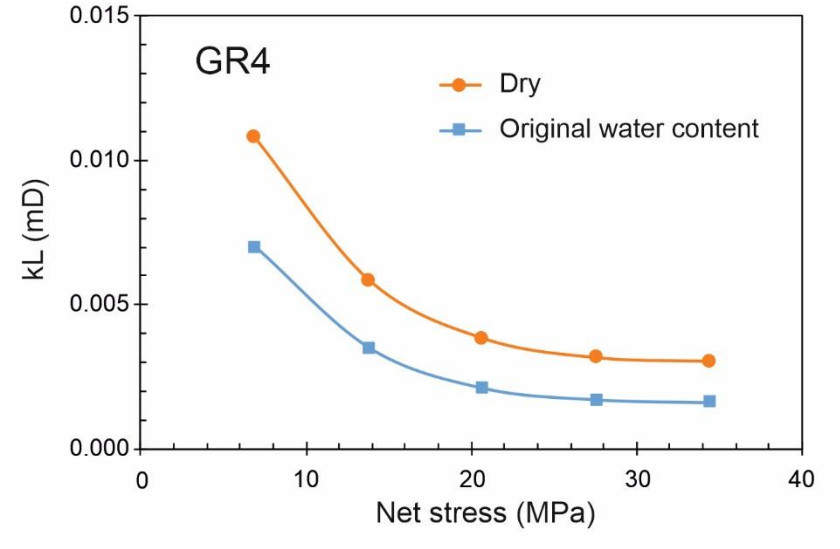

Figure 8